Polarization of acetonitrile under thermal fields via non-equilibrium molecular dynamics simulations

Oliver R. Gittus,[1, a)] Pablo Albella,[2, b)] and Fernando Bresme[1, c)]
[1)] *Department of Chemistry, Molecular Sciences Research Hub Imperial College, W12 0BZ, London, United Kingdom*
[2)] *Department of Applied Physics (Group of Optics), University of Cantabria, Avda. Los Castros, s/n, Santander, 39005, Spain*

(Dated: 16 December 2020)

We show that thermal gradients polarize liquid and supercritical acetonitrile. The polarization results in a stationary electrostatic potential that builds up between hot and cold regions. The strength of the field increases with the static dielectric constant or with decreasing temperature. At near standard conditions the thermal polarization coefficient is ~ -0.6 mV/K, making it possible to induce significant electrostatic fields, $\sim 10^3$ V/m, with thermal gradients ~ 1 K/μm. At supercritical conditions, $\sim$600 K and 0.249 g/cm^3 (the critical isochore), the electrostatic field is of the same order, despite the low dielectric constant of the fluid. In this case the electrostatic field is determined by the enhanced rotational diffusion of the molecules, and stronger cross-coupling between heat and polarization fluxes. We show that the coupling between the heat and polarization fluxes influences the thermal conductivity of acetonitrile, which becomes a worse heat conductor. For the thermodynamic states investigated in this work, the thermal polarization effect leads to a $\sim$2-5 % reduction in thermal conductivity.

I. INTRODUCTION

Temperature gradients are ubiquitous in Nature and industry. There is an ongoing interest in the use of thermal gradients to induce thermophoretic transport in solutions, or to recover waste heat. The application of a thermal gradient to an ionic solution induces a concentration gradient, the Soret effect, and electrostatic potential, the Seebeck effect. In addition to these coupling effects between heat, charge and mass fluxes, it has been demonstrated that water becomes polarized when exposed to a thermal flux. This phenomenon, called thermal polarization[1], increases linearly with the magnitude of the thermal gradient, and in the case of water has been shown to be particularly strong at super-critical conditions[2]. Thermal polarization, or more generally thermal orientation, has also been observed in models of simple polar fluids[3–5], as well as non-polar fluids[6,7] and colloids[8], when the particles are anisotropic in mass and/or size.

Although most investigations to date dealing with real molecular fluids have focused on water, thermal polarization should also be observed in other highly polar fluids. Examining the response and physical behavior of different fluids is necessary to explain more generally the behavior of polar fluids under thermal fields, and the first step in rationalizing correlations between thermal polarization and molecular structure. Moreover, this understanding might inspire avenues for applications. Thermal orientation effects have been discussed in the electroporation of biological membranes[9], the dynamical ordering of quantum fluids[10] and the generation of thermal monopoles[5]. The importance of these effects in other polar fluids have, however, not been fully addressed.

In this work we investigate the thermal polarization effect in acetonitrile (ACN). ACN is a highly polar fluid, which is widely used as aprotic solvent in synthesis and energy applications. ACN also features a strong response to electromagnetic fields, e.g. the Optical Kerr Effect, with a Kerr constant about half that of o-nitrotoluene, which is amongst the liquids featuring the strongest birefrigence response[11]. Shelton[12] measured the depolarized hyper-Rayleigh scattering spectra of ACN. The results were interpreted as indicative of a ferroelectric transition with the formation of small ferroelectric domains. This motivated computer simulation studies to test the existence of such domains[13]. It was concluded that acetonitrile does not feature local ferroelectric domains, in disagreement with the conclusions of the experimental studies. However, these investigations were performed under equilibrium conditions. The impact of transient or stationary thermal fields on ACN is unknown.

Thermal gradients have been shown to induce polarization in liquid water. This coupling phenomenon can be formalized with Non-Equilibrium Thermodynamics theory, and described in terms of phenomenological coefficients and the dielectric permittivity. This phenomenon depends on the general properties of polar fluids, and we therefore expect it will be present in acetonitrile as well. In this work, we investigate the thermal polarization of acetonitrile, and quantify the strength of the effect at standard and supercritical conditions. Furthermore, we quantify the reduction in the thermal conductivity of ACN, as induced by the thermal polarization effect.

[a)] Electronic mail: o.gittus18@imperial.ac.uk
[b)] Electronic mail: pablo.albella@unican.es
[c)] Electronic mail: f.bresme@imperial.ac.uk

II. METHODS

We performed equilibrium and non-equilibrium molecular dynamics simulations of acetonitrile at thermodynamic conditions ranging from standard to supercritical. Acetonitrile molecules were modelled as rigid bodies using the TraPPE force field (see Fig. 1C), which predicts thermophysical properties in good agreement with experimental results[14].The molecule is modelled using a united atom representation and rigid bonds. The equations of motion were integrated using the velocity Verlet algorithm and a standard timestep of 2 fs. Rigid body dynamics were evolved using two virtual sites located along the ACN axis[15,16], whose distance was kept constant using the LINCS algorithm[17]. The coordinates of the CH_3, C and N interaction sites were represented relative to the position of these virtual sites, such that the total force and the total torque are conserved[15,16]. Electrostatic interactions were calculated using the Particle Mesh Ewald method[18]. A cutoff of 1.06 nm was used for the dispersion interactions. All trajectories were generated with the code Gromacs v. 2020.[16,19]

Boundary-driven non-equilibrium molecular dynamics (NEMD) simulations, using a restraint approach was used to model the fluids in the stationary state. An orthorhombic simulation cell of dimensions $(L_x, L_y, L_z) = (3.564, 3.564, 35.639)$ nm was used, with 3D periodic boundary conditions. The two thermostatting regions, hot and cold, were located in the centre and edges of the box, respectively (see Fig. 1). The thermostatting regions extend in the (x, y) plane, such that the temperature gradients are generated along the z-direction. In the stationary state, this set-up results in two equal but opposite temperature gradients, and therefore in equal and opposite heat fluxes, such that the system is completely periodic.

The thermostats were applied, every timestep, to acetonitrile molecules located in the thermostatting regions. We restrained the position of the carbon atom bonded to nitrogen to its initial z-coordinate using a harmonic potential with a force constant of 10^3 kJ mol^{-1} nm^{-2}. The restraint was applied only in the z-direction: the molecules were free to rotate, and also translate in the x- and y-directions. The temperature difference between the hot and cold thermostats was set to 100 K for all the NEMD simulations reported in this work.

The thermostatting process was implemented using the Nosé-Hoover thermostat, which reproduces the canonical (NVT) ensemble. A single thermostat was applied to each of the thermostatting regions only, using one chain, while the trajectories of all other molecules were generated following standard Newtonian dynamics. The Nosé-Hoover equations include an equation of motion for the dynamic variable p_ξ, which models the dynamic exchange of heat of the system at temperature T, with a reservoir

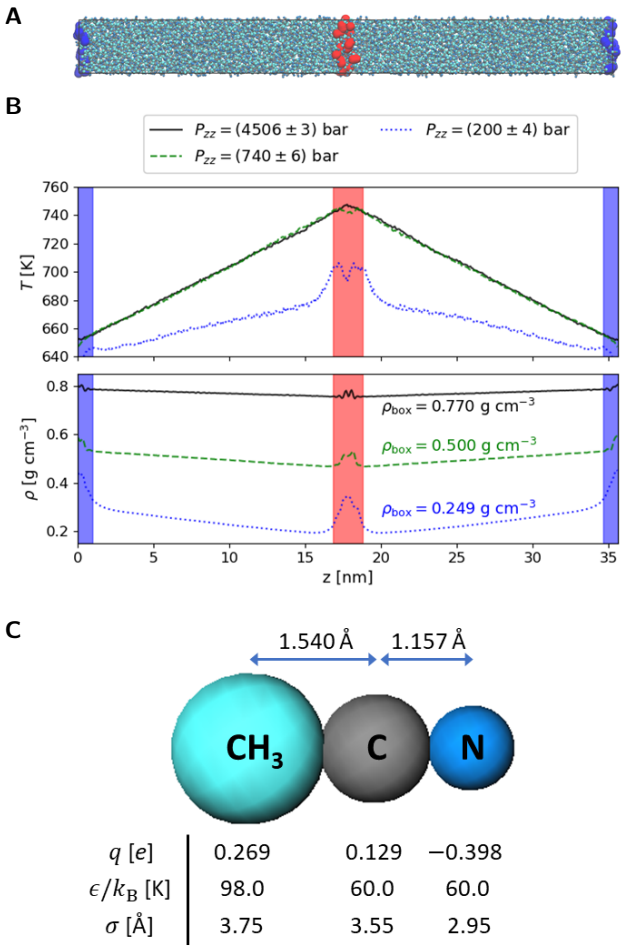

	CH_3	C	N
q [e]	0.269	0.129	−0.398
ϵ/k_B [K]	98.0	60.0	60.0
σ [Å]	3.75	3.55	2.95

FIG. 1. Non-equilibrium molecular dynamics simulation set-up. (A) Snapshot of the simulation box: thermostat regions are represented by enlarged red (hot) and cold (blue) molecules; acetonitrile molecules are comprised of C atoms (grey), N atoms (sky blue) and CH_3 groups (cyan). (B) Representative temperature (middle) and density (bottom) profiles for the systems investigated in this work. The blue (cold) and red (hot) shaded areas indicate the location of the thermostats in the simulation box. Average simulation cell densities are shown next to the corresponding density profile. The density profiles include all the molecules in the system, while the temperature profiles exclude the restrained molecules used to thermostat the system in the hot and cold regions. The pressure tensor component P_{zz} parallel to the heat flux vector is shown in the legend for each profile. (C) Graphical representation of the TraPPE force field of acetonitrile. The charge q and Lennard-Jones parameters ϵ and σ are shown under their corresponding species, while rigid bond distances are shown above the molecule. The same colour coding as in (A) is used.

that is set to the desired temperature T_r:

$$\frac{d\mathbf{v}_i}{dt} = \frac{\mathbf{f}_i}{m_i} - \frac{p_\xi}{Q}\mathbf{v}_i \quad (1)$$

$$\frac{dp_\xi/Q}{dt} = \frac{(T - T_r)}{Q} \quad (2)$$

where $Q = \tau_T^2 T_r/(4\pi^2)$, τ_T defines the period of the temperature fluctuations, which was set to 1 ps. $\mathbf{v}_i$ and $\mathbf{f}_i$ are the velocity and the force acting on particle i with mass m_i. The Nosé-Hoover Hamiltonian incorporates the contributions due to the reservoir:

$$H(\mathbf{r}^N, \mathbf{p}, \xi) = \sum_{i=1} \frac{\mathbf{p}_i^2}{2m_i} + U(\mathbf{r}^N) + \frac{p_\xi^2}{2Q} + N_{dof} k_B T \xi \quad (3)$$

where $\mathbf{r}^N = (\mathbf{r}_1, \mathbf{r}_2, \cdots, \mathbf{r}_N)$, $\dot{\xi} \equiv \mathrm{d}\xi/dt = p_\xi/Q$ and N_{dof} is the total number of degrees of freedom of the region being thermostatted. The last two terms in Eq. (3) represent the energy exchanged with the reservoir. The heat flux, $\boldsymbol{J}_q = (0, 0, \pm J_q)$, can be obtained from the time-average value of $\dot{\xi}$ using the continuity equation:

$$J_q = -\frac{\langle\dot{\xi}\rangle N_{dof} k_B T}{A} \quad (4)$$

where $A = (L_x \times L_y)^2 = 3.564^2$ nm^2 ($L_x \equiv L_y$) is the cross sectional area of the simulation box. The simulations were performed with systems consisting of 1590-5050 molecules to target different densities (see Fig. 2 and Table 1 for a summary of the systems investigated in this work). Each thermostat was coupled to 33 molecules, giving $N_{dof} = 165$ (5 degrees of freedom per molecule). Similar numbers of molecules were used in our previous NEMD simulations, providing well defined heat fluxes and thermal gradients[2].

After the stationary state was reached, each NEMD simulation involved trajectories of either 4 ns or 8 ns. Longer trajectories were used for the low density systems. To ensure good statistics, for each state point we simulated several replicas, 5 for high densities, and up to 25 (200 ns of sampling) for low densities ($\rho = 0.249$ g cm^{-3}). The fluctuations for these low density systems are large, particularly as the critical temperature is approached. Extensive sampling was needed to obtain averages within acceptable statistical uncertainty. The profiles were computed using 500 bins. The mass and charge densities were obtained by assigning each atom to its corresponding bin. The electrostatic field was obtained from the integration of the charge density

We also performed equilibrium simulations in the isothermal-isobaric (NPT) ensemble[20] to test the equation of state obtained from NEMD. Simulations in the canonical (NVT) ensemble using the CSVR[21] (v-rescale) thermostat were performed in order to compute: (1) coexistence lines from simulations of explicit liquid-vapour interfaces, using the direct coexistence method[22]; and (2) dielectric properties and Debye relaxation times. A typical simulation consisted of 1000 molecules, 1 ns of equilibration time and 9 ns of production, with typically 6-10 statistically independent replicas. We employed a smaller timestep, 1 fs, to calculate the dipole moment correlation functions.

III. RESULTS

The thermodynamic states investigated in this work are shown in Fig. 2. We targeted the standard state, high temperature/density systems, and states along the critical isochore. It has previously been shown that the TraPPE force field accurately reproduces the phase diagram of acetonitrile, including the critical point.[14] Our coexistence densities, obtained using the direct coexistence method, are in good agreement with these previous simulations[14] . With regards to the NEMD data, we show in Fig. 1 representative temperature and density profiles for selected thermodynamic states. Only spatial bins located at least 4 nm from the centre and edges of the simulation cell were used, in order to exclude any possible artefacts arising from the thermostats. Each set of profiles corresponds to the equation of state (EOS) at the simulated pressure, as defined by the component (P_{zz}) parallel to the heat flux vector. The EOS obtained from NEMD (see Fig. 2) reproduces the behavior of the fluid at equilibrium. This is equivalent to stating that the NEMD simulations generate a collection of states that fulfill local equilibrium, a key assumption in Linear Non-Equilibrium Thermodynamics. We demonstrate that this is the case in the inset of Fig. 2. In all cases, the NEMD simulations employed temperature gradients between 1-5 K nm^{-1}. This magnitude for the thermal gradient is widely used in computer simulations, as it provides a small noise to signal ratio, making it feasible to compute the thermal polarization[1]. Although experimental setups at the micro and nanoscale are approaching gradients of this magnitude[23,24], the simulated gradients are large by macroscopic standards. However, the good agreement between NEMD and equilibrium-NPT results indicates that the response of our systems is in the linear regime, and that the local equilibrium hypothesis is fulfilled by our simulations. This observation agrees with previous conclusions using different molecular fluids[2].

We have demonstrated above that locally the NEMD simulations reproduce the equation of state of the fluids. We took advantage of this to calculate the thermal conductivity of acetonitrile at different thermodynamic conditions using Fourier's law ($\lambda = -\boldsymbol{J}_q/\nabla T$) and the local temperature gradient, at the temperature and density of interest. The temperature gradient was determined by fitting a straight line to the temperature profile within a range of ± 2 nm around the selected state point. We note that the computation of the thermal conductivity via NEMD includes all possible coupling effects (e.g. those arising from mass-heat flux coupling[25]). We discuss later in this work the coupling between heat and polarization fluxes and how it influences the thermal conductivity of

TABLE I. Thermodynamics states simulated in this work using non-equilibrium molecular dynamics. ρ_{box}, T_{box}, P_{zz}, represent the average density, temperature and pressure parallel to the direction of the heat flux, respectively. T_h and T_c are the temperatures of the hot and cold thermostats, λ is the thermal conductivity, S_{TP} is the thermal polarization coefficient, and E and E_P are the total electrostatic field and the dipolar contribution to the total field, respectively. All local properties (columns 8-12) were computed at the thermodynamics conditions specified by density ρ and temperature T. Statistical uncertainties (standard error of the mean) in the least significant figure are given in parenthesis.

ρ_{box}	T_c	T_h	T_{box}	P_{zz}	ρ	T	∇T	λ	S_{TP}	E	E_P
[g cm^{-3}]	[K]	[K]	[K]	[bar]	[g cm^{-3}]	[K]	[K nm^{-1}]	[W/(K m)]	[mV K^{-1}]	[mV nm^{-1}]	[mV nm^{-1}]
0.770	255	355	302	43(8)	0.770	303	4.9(1)	0.239(7)	-0.56(6)	-2.7(3)	-2.5(3)
0.770	350	450	397	1205(6)	0.770	397	5.3(1)	0.229(5)	-0.41(6)	-2.2(3)	-1.8(3)
0.770	450	550	498	2400(20)	0.770	498	5.4(1)	0.236(5)	-0.34(6)	-1.8(3)	-1.6(4)
0.770	550	650	599	3470(10)	0.770	598	5.2(2)	0.246(9)	-0.32(7)	-1.6(3)	-1.2(4)
0.770	650	750	698	4506(3)	0.770	697	5.5(2)	0.234(9)	-0.21(6)	-1.1(3)	-0.8(3)
0.350	650	750	699	353(4)	0.333	700	4.9(2)	0.072(3)	-0.07(3)	-0.3(1)	-0.1(2)
0.500	650	750	698	740(6)	0.495	700	5.4(2)	0.109(4)	-0.16(3)	-0.8(2)	-0.7(2)
0.650	650	750	704	2037(4)	0.650	700	5.3(1)	0.179(4)	-0.18(2)	-0.9(1)	-0.5(1)
0.249	600	700	637	104(1)	0.249	607	0.99(8)	0.26(2)	-0.3(1)	-0.3(1)	0.2(1)
0.249	605	705	644	109(2)	0.249	613	1.18(6)	0.21(1)	-0.19(8)	-0.22(9)	0.32(9)
0.249	620	720	660	124(2)	0.249	627	1.74(9)	0.144(8)	-0.12(7)	-0.2(1)	0.3(1)
0.249	630	730	671	133(1)	0.249	638	2.07(9)	0.121(5)	-0.15(5)	-0.3(1)	0.1(1)
0.249	640	740	681	142(2)	0.249	648	2.40(9)	0.106(4)	-0.09(4)	-0.20(9)	0.2(1)
0.249	650	750	692	151(2)	0.249	658	2.7(1)	0.097(6)	-0.10(5)	-0.3(1)	0.1(1)
0.249	660	760	703	159(2)	0.249	667	3.0(1)	0.088(4)	-0.10(5)	-0.3(1)	0.0(1)

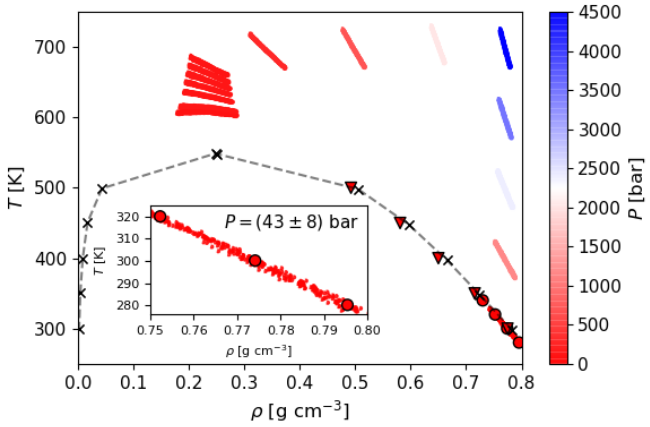

FIG. 2. Thermodynamic states investigated in this work with reference to the coexistence curve of acetonitrile. Literature values from previous simulations[14] are represented as crosses with dashed lines (--×). The coloured triangle-down (▽) symbols along the coexistence line represent coexistence densities obtained in this work using the direct coexistence method. We also show the temperature/density data obtained from the NEMD simulations (dots (·), which may appear as thick lines) Our data is colour coded according to the pressure of the system. The inset compares the equation of state obtained from NEMD at $P = (43 \pm 8)$ bar (dots (·)), and the data obtained from equilibrium (NPT) simulations at the same pressure (circles (○)).

acetonitrile.

The thermal conductivities computed in this work are shown in Table I and Fig. 3. The TraPPE force field predicts $\lambda = (0.239 \pm 0.007)$ W K^{-1} m^{-1} at 303 K and 0.770 g cm^{-3}, corresponding to a pressure of $P = (43 \pm 8)$ bar. This result is on the order of the thermal conductivity reported experimentally at 293.15 K and ambient pressure: 0.195 W K^{-1} m^{-1} and 0.2034 W K^{-1} m^{-1}.[26,27] In the latter case, a density of 0.7897 g cm^{-3} was also reported.[27] Note that it is also comparable to the experimental value of 0.183 W K^{-1} m^{-1} obtained at 313.15 K at ambient pressure.[26]

As shown in Fig. 3 the thermal conductivity does not change significantly with temperature along the 0.770 g cm^{-3} isochore. In contrast, the critical isochore features a strong increase with temperature as the critical point is approached. This behavior is consistent with the enhancement discussed previously by Sengers[28]. We have not attempted to fit our data to a power law since our temperatures are well above the critical temperature. Moving along the $T = 700$ K isotherm, we observe an increase in thermal conductivity with density (see Fig. 3B).

Previous studies demonstrated that thermal fields polarize liquid water.[1] It follows from Linear Non-Equilibrium Thermodynamics that *thermal polarization* (TP) is a general effect in polar fluids, and should therefore be observed in acetonitrile. We summarize the main ideas in the following. The application of a thermal gradient, ∇T, induces an electrostatic field $\boldsymbol{E}$, given by:[1]

$$\boldsymbol{E} = \left(1 - \frac{1}{\varepsilon_r}\right) \frac{L_{pq}}{L_{pp}} \frac{\nabla T}{T} \tag{5}$$

where ε_r is the static dielectric constant of the fluid, and $L_{\alpha\beta}$ are the phenomenological coefficients, with L_{pq} measuring the strength of the heat-polarization coupling, and L_{pp} is connected to the relaxation time of the polarization (see below) . Equation (5) predicts an increase of the TP response with the dielectric constant of the fluid, the

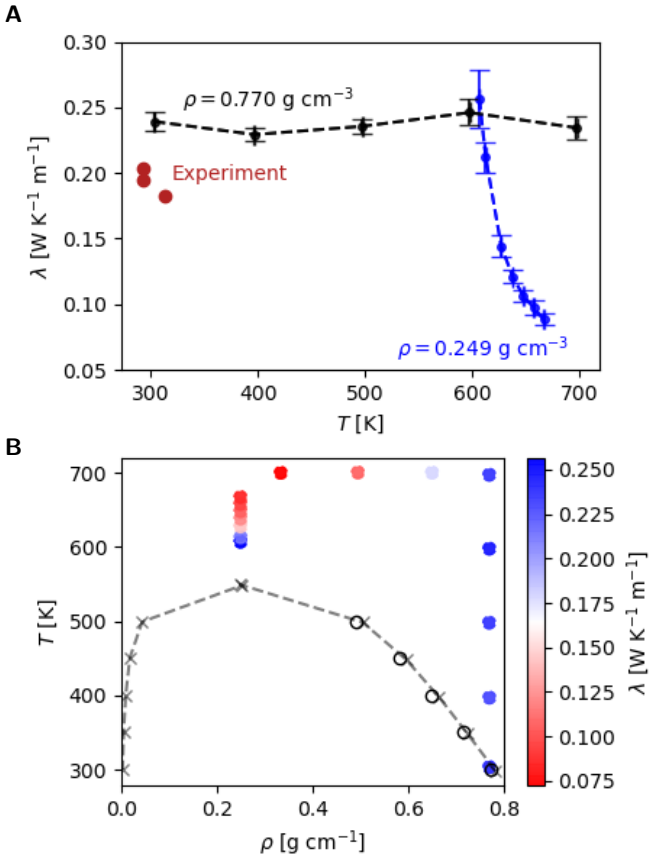

FIG. 3. Thermal conductivity λ of acetonitrile computed in this work using the TraPPE force field. (A) The high density (ρ = 0.770 g cm^{-3}) and critical (ρ = 0.249 g cm^{-3}) isochores, along with experimental values measured at ambient pressure (see text for discussion). (B) Thermal conductivities with reference to the phase diagram of acetonitrile. The data is colour coded according to the magnitude of the thermal conductivity.

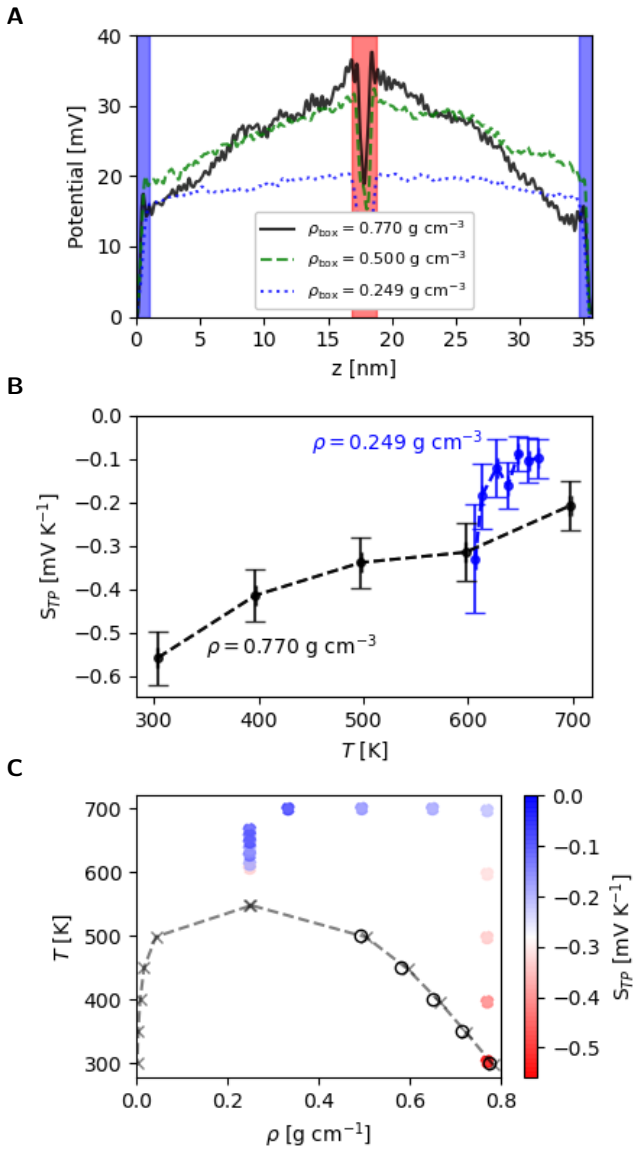

FIG. 4. Thermal polarization of acetonitrile from NEMD simulations. (A) Electrostatic potential across the simulation box for representative systems at different densities. The corresponding temperature and density profiles are shown in Fig. 1. Thermal polarization coefficient S_{TP} for (B) high density (ρ = 0.770 g cm^{-3}) and critical (ρ = 0.249 g cm^{-3}) isochores, and (C) with reference to the phase diagram of acetonitrile. In (C), the data is colour coded according the value of S_{TP}.

ratio L_{pq}/L_{pp} and the thermal gradient, and a decreases with temperature. The strength of the TP effect can be quantified using the *thermal polarization coefficient*, $S_{TP} = E/\nabla T$.[2]

The phenomenological coefficient L_{pp} appearing in Eq. (5) is related to the Debye relaxation time, τ, via:[29]

$$\boldsymbol{P}(t) = \kappa \boldsymbol{E}\,(1 - \exp(-t/\tau)) \tag{6}$$

where $\boldsymbol{P}$ is the polarization, which in the absence of free charges is given by $\boldsymbol{P} = -\epsilon_0 \boldsymbol{E}$, and $\kappa = (\varepsilon_r - 1)\varepsilon_0$. The phenomenological coefficient is then defined as:

$$L_{pp} = \frac{\kappa T}{\tau}, \tag{7}$$

hence providing an approximation to obtain L_{pp} within the assumptions used in the Debye model. Once L_{pp} is known, it is possible to extract L_{pq} from Eq. (5), provided $\boldsymbol{E}$, ε_r, ∇T and T are known. All these quantities are either defined in our simulation set-up (∇T and T) or are accessible through NEMD or equilibrium simulations ($\boldsymbol{E}$, ε_r).

The electrostatic field induced by the thermal gradient was calculated by integrating the total charge density along the direction of the heat flux,

$$E(z) = \frac{1}{\varepsilon_0} \int_0^z \rho_q(z')dz' \tag{8}$$

where ε_0 is the vacuum permittivity, and $\rho_q(z)$ =

$\left(\sum_{i=1}^{N}\delta(z-z_i)q_i\right)/A$ is the charge density, A being the cross sectional area of the simulation box. The sum runs over all N charges in the system. We also calculated the dipolar field, E_P (see ref. 2),

$$E_P(z) = \frac{-1}{\varepsilon_0}\int_0^z \frac{dP_z(z')}{dz'}dz', \tag{9}$$

with

$$P_z(z) = \frac{1}{A}\left\langle \sum_{i=1}^{N_m}\delta(z-z_i)\left[\sum_{j=1}^{j\in m} q_{j,m}z_{j,m}\right]\right\rangle \tag{10}$$

where the first and second sums in Eq. (10) run over the number of molecules N_m, and the number of atoms in molecule m, respectively, and for z_i we used the position of the central atom in each molecule. The calculation of the total and dipolar fields allows us to assess the importance of higher order terms in determining the strength of the thermal polarization field. In the case of water, the higher order terms were found to dominate the electrostatic response at high temperatures and low densities, when the fluid features a larger thermal expansion. The balance of these contributions results in a change in the sign of the thermally induced electrostatic field, and therefore in S_{TP} when the liquid is heated.[2]

We compile in Table I the NEMD results for the electrostatic field induced by the thermal field at different thermodynamic conditions. The simulations confirm the generality of the TP effect. A clear polarization field across the simulation box is observed, as evidenced by the slope of the potentials shown in Fig. 4(A).

The strength of the TP effect depends on the thermodynamic conditions, density and temperature, highlighting the dependence of the phenomenological coefficients with these properties. At high densities, $\rho = 0.770$ g cm^{-3}, the polarization is strongest at near standard conditions, and decreases with temperature: by ∼60% from 300 K to 700 K. Similarly, $|S_{TP}|$ decreases with temperature along the critical isochore, decreasing by ∼70% from 600 K to 660 K. The enhancement in TP as the system approaches the critical temperature resembles the behavior reported previously for water[2]. At 607 K ($T/T_c - 1 \sim 0.1$), $S_{TP} = -(0.3 \pm 0.1)$ mV K^{-1} (see Table I) has a similar magnitude to that near standard conditions. This value is one order of magnitude lower than that obtained for water at the same $T/T_c - 1$, −2.5 mV K^{-1},[2] highlighting differences in the TP response of these two polar fluids. We also note that $|S_{TP}|$ increases with density along the $T = 700$ K isotherm: by ∼200% from 0.333 g cm^{-3} to 0.770 g cm^{-3}.

For all the systems investigated in this work, the thermal polarization coefficient of acetonitrile is negative, $S_{TP} < 0$. This is in contrast with the TP effect in water, where a field inversion is observed.[2] This inversion phenomenon in water is connected to the balance of dipolar and quadrupolar contributions to the electrostatic field, with the latter changing significantly with the thermodynamic conditions. We report in Fig. 5 the dipolar and higher order contributions to the total thermal polarization field of acetonitrile. At high densities, $\rho = 0.770$ g cm^{-3}, the dipolar term is negative for all temperatures investigated, and is the dominant contribution (∼70-90%, noting the high uncertainties of ∼10-30% associated with these percentages) to the total field. $E_P < 0$ indicates that the molecules orient preferentially with the dipole pointing toward the hot region. The small impact of higher order terms in defining the field explains the lack of inversion in the TP field at this high density. Along the critical isochore the situation is more complex. In all cases, $E_P > 0$ (or straddles 0 given the uncertainty) indicating that the molecules orient preferentially with the dipole pointing toward the cold. Our results indicate that at high temperatures, the dipolar and higher order term contributions have similar values, but opposite signs, while the higher order terms dominate the TP response upon approaching the critical temperature. This result follows previous observations for water, where contributions beyond the dipolar term became dominant near critical conditions, mirroring the increase of the thermal expansion coefficient.[2]

Next, we briefly consider the relative importance of the parameters given in Eq. (5) to S_{TP}. As shown in Table II, ε_r features only a weak dependence with temperature: at a density of $\rho = 0.770$ g cm^{-3} ($\rho = 0.249$ g cm^{-3}), ε_r decreases by ∼8% (∼ 1%) from 300 K to 700 K (610 K to 670 K), while S_{TP} changes by ∼60% (∼70%). These small changes in ε_r correspond to even smaller differences of $< 1\%$ in $(1 - 1/\varepsilon_r)$. Since TS_{TP} is not constant with T, S_{TP} must be interpreted in terms of changes in both T and L_{pq}/L_{pp}. We address the latter in the following, by calculating L_{pq} and L_{pp}.

The phenomenological coefficients can be obtained using Eqs. (5) and (7). To calculate L_{pp} we computed the static dielectric constant ε_r, and Debye relaxation time τ of acetonitrile. ε_r was calculated from the analysis of the total dipolar fluctuations in the simulation box:

$$\varepsilon_r - 1 = \frac{\left\langle \mathbf{P}^2\right\rangle - \left\langle \mathbf{P}\right\rangle^2}{3Vk_BT\varepsilon_0}, \tag{11}$$

where $\mathbf{P} = \sum_{i=1}^{N} q_i\mathbf{r}_i$, V is the volume of the simulation box and the brackets <> indicate a time average. The Debye relaxation time τ was calculated from the normalized total dipole moment correlation functions: $\langle \mathbf{P}(t)\cdot\mathbf{P}(0)\rangle / \langle \mathbf{P}(0)\cdot\mathbf{P}(0)\rangle$ and $\frac{1}{N_m}\sum_{i=1}^{N_m}\langle \mathbf{p}(t)\cdot\mathbf{p}(0)\rangle / \langle \mathbf{p}(0)\cdot\mathbf{p}(0)\rangle$ respectively, where $\mathbf{p}$ is the dipole moment vector of a single molecule. The dielectric constants were computed using trajectories spanning 9 ns (see Fig. 6(A)), with 6-11 statistically independent replicas to calculate averages and associated uncertainties. The dipole-dipole total and molecular correlation functions were computed using the same trajectories. The resulting correlation functions feature a typical exponential decay. We fitted the initial decay of the correlation functions to a single exponential curve

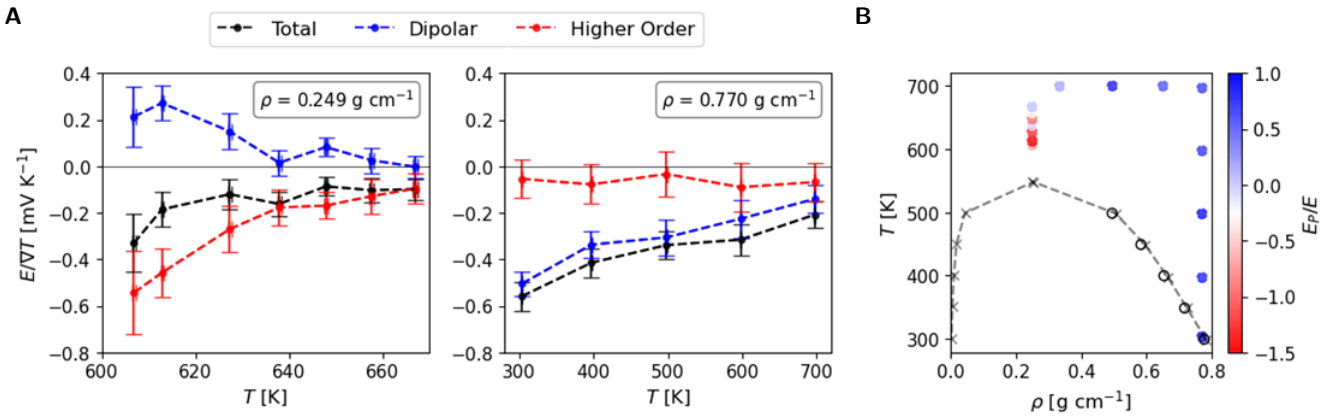

FIG. 5. (A) Contributions to the electrostatic field for the (left) critical isochore (0.249 g cm^{-3}) and (right) high density states (0.770 g cm^{-3}). For a fair comparison, the reduced field $S_{TP} = E/\nabla T$ has been reported. (B) The ratio of dipolar contribution E_P to the total electrostatic field E, with reference to the phase diagram of acetonitrile. The data is colour coded according to the ratio E_P/E.

$f(t) = A\exp(-t/\tau_\alpha)$, with an upper cutoff for the fitting of 5 and 2 ps, for high (0.770 g cm^{-3}) and low (0.249 g cm^{-3}) density states respectively. The exception to this is the (ρ, T) = (0.770 g cm^{-3}, 697 K) point, with a cutoff of 3.5 ps. This model assumes the simplest treatment considering a single relaxation time, consistent with Eq. (6).

Our results for the dielectric constant and dipolar correlation times are reported in Table II. At 303 K and 0.770 g cm^{-3} the simulated dielectric constant is close to the experimental value,[30] with a relative deviation -13%, which is acceptable considering the simplicity of the model and slight difference in thermodynamic conditions. The Debye relaxation time is also consistent with experimental estimates of 3.5 ps[30] and 3.7 ps[31]. Similar relaxation times are obtained using the total (τ_P) or molecular (τ_p) dipole moments, indicating a small impact from cross correlations. τ_p values are systematically lower. At high density, increasing the temperature results in a small decrease of the dielectric constant, while the relaxation time becomes significantly shorter. This is expected, as the rotational diffusion increases with temperature. The dielectric constant is much smaller along the critical isochore, and changes only marginally for the temperature interval investigated. These supercritical states feature shorter relaxation times for dipole correlations, ~ 0.5 ps, as expected given the higher temperatures.

The results discussed above show that the acetonitrile model employed here predicts dielectric properties in good agreement with experiments. We use this data together with our S_{TP} values, to estimate the phenomenological coefficients L_{pp} and L_{pq}. L_{pp} was obtained from Eq. (7) using the τ_P values reported in Table II. L_{pq} can be obtained from the following equation:

$$S_{TP} = \left(1 - \frac{1}{\varepsilon_r}\right)\frac{L_{pq}}{L_{pp}}\frac{1}{T}, \qquad (12)$$

where S_{TP} is calculated directly from the NEMD results

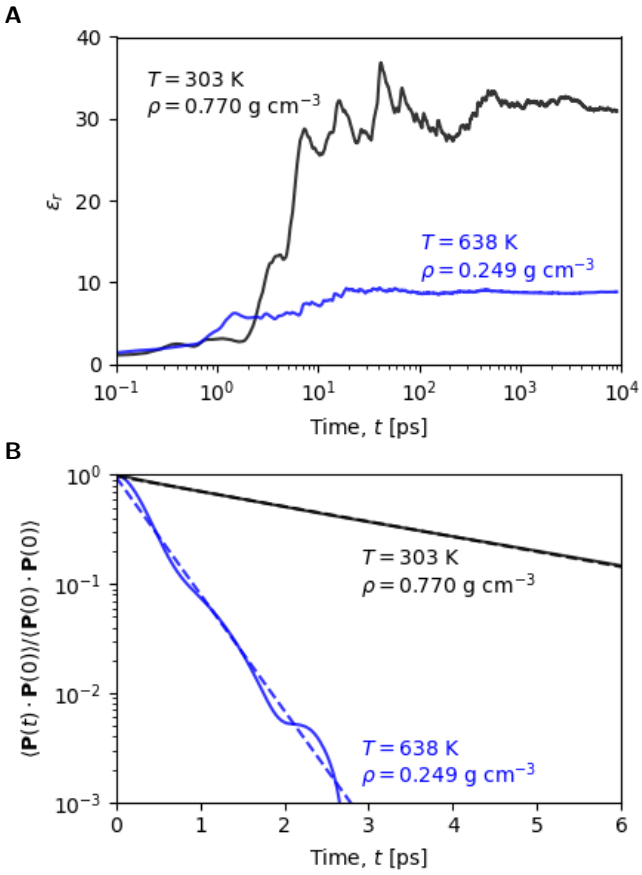

FIG. 6. Dielectric properties of acetonitrile from equilibrium-NPT simulations. (A) Convergence of the dielectric constant ε_r with time t for the thermodynamics states (ρ, T)=(0.770 g cm^{-1}, 303 K) and (0.249 g cm^{-1}, 638 K). (B) Total dipole correlation functions, $\langle \mathbf{P}(t)\cdot\mathbf{P}(0)\rangle / \langle \mathbf{P}(0)\cdot\mathbf{P}(0)\rangle$, for the same thermodynamic states. Dotted lines represent the fit to the exponential function $f(t) = A\exp(-t/\tau_P)$.

TABLE II. Dielectric properties, phenomenological coefficients and thermal conductivities of acetonitrile at selected thermodynamic conditions (density ρ and temperature T): static dielectric constant ε_r; dipolar relaxation times calculated using the total τ_P and averaged molecular τ_p dipole moment vectors; L_{pp} and L_{pq} are the phenomenological coefficients; $\delta\lambda$ is the difference between the total thermal conductivity λ and that in the absence of the thermal polarization coupling effect $\lambda_{L_{pq}=0}$. Statistical uncertainties (standard error of the mean) in the least significant figure are given in parenthesis.

ρ	T	ε_r	τ_p	τ_P	$L_{pp}\times10^{-4}$	$L_{pq}\times10^{-4}$	L_{pq}/L_{pp}	λ	$\lambda_{L_{pq}=0}$	$\delta\lambda$	$\delta\lambda$
[g cm^{-3}]	[K]		[ps]	[ps]	[C^2 K/(J m s)]	[C K/(m s)]	[V]	[W/(K m)]	[W/(K m)]	[W/(K m)]	[%]
0.770	303	31.3(1)	3.061(2)	3.13(2)	2.59(2)	-0.45(5)	-0.18(2)	0.239(7)	0.248(7)	-0.009(2)	-3.6(8)
0.770	498	30.0(1)	1.462(1)	1.51(3)	8.5(1)	-1.5(3)	-0.17(3)	0.236(5)	0.246(6)	-0.010(4)	-4(2)
0.770	697	28.94(9)	0.929(1)	0.98(2)	17.6(3)	-2.6(7)	-0.15(4)	0.234(9)	0.24(1)	-0.008(4)	-3(2)
0.249	607	8.78(1)	0.367(1)	0.47(1)	8.9(2)	-2.0(8)	-0.23(9)	0.26(2)	0.27(2)	-0.012(9)	-5(4)
0.249	638	8.81(2)	0.348(1)	0.42(2)	10.5(4)	-1.2(4)	-0.12(4)	0.121(5)	0.125(6)	-0.004(2)	-3(2)
0.249	667	8.84(2)	0.325(1)	0.40(1)	11.6(4)	-0.9(4)	-0.07(3)	0.088(4)	0.090(5)	-0.001(1)	-2(1)

(Table I). Values for the two phenomenological coefficients are collected in Table II. The coefficients depend strongly on the temperature. In the case of L_{pp}, the rapid increase with temperature is due to the significant speed-up of rotational dynamics, reflected in shorter relaxation times, τ_P. Interestingly, $|L_{pq}|$ increases with temperature at 0.770 g cm^{-3}, but decreases with temperature along the critical isochore as one moves away from the critical temperature. At both densities, the ratio $|L_{pq}/L_{pp}|$ decreases with temperature; however, the values in each isochore overlap considering their associated statistical uncertainty. As mentioned previously, the S_{TP} coefficients at (607 K, 0.249 g cm^{-3}) (approximately 10% above the critical point) and (303 K, 0.770 g cm^{-3}), are similar. The ratio $|L_{pq}/L_{pp}|$ in Eq. (12) in the supercritical states is about 30% larger than that of the low temperature/high density system. For the latter system, the strong polarization response is driven by a significantly higher dielectric constant and lower temperature, which enhance the TP effect (see Eq. (12)).

The phenomenological coefficients can be used to assess the impact of the TP effect on the thermal conductivity. It is well established that coupling effects impact transport properties, for example the Soret effect, where heat-mass flux coupling decreases the thermal conductivity.[25,29] However, the impact of TP remains unexplored. In this case, the thermal conductivity can be written in terms of the phenomenological coefficients[1]:

$$\lambda = \frac{1}{T^2}\left(L_{qq} - \frac{L_{pq}L_{qp}}{L_{pp}}\right) \tag{13}$$

where L_{qq} is the phenomenological coefficient associated with the heat flux and $L_{pq} \equiv L_{qp}$ are the cross-coupling coefficients. Following Non-Equilibrium Thermodynamics $L_{qq}L_{pp} - L_{pq}^2 \geq 0$, hence $L_{pq} \neq 0$ implies that the TP coupling effect should always decrease λ. The thermal conductivity values were obtained directly from our NEMD simulations using Fourier's law and local thermal gradients, calculated for the densities and temperatures of interest (see Table I). Hence the NEMD thermal conductivities include all possible non-equilibrium effects, in our case the TP coupling. Equation (13) thus provides a route to estimate the reduction of the thermal conductivity associated with the cross-coupling of heat and polarization fluxes. When $L_{pq} = 0$ such coupling does not exist, and we obtain the corresponding thermal conductivity, $\lambda_{L_{pq}=0}$. Thus, one can write: $\lambda = \lambda_{L_{pq}=0} + \delta\lambda$, where we compute $\delta\lambda = -\frac{1}{T^2}\frac{L_{pq}^2}{L_{pp}}$ directly from variables T, S_{TP}, τ_P and ε_r, according to

$$\delta\lambda = -\frac{S_{TP}^2 T}{\tau}\left(\frac{\varepsilon_0\varepsilon_r^2}{\varepsilon_r - 1}\right) \tag{14}$$

Our results for $\delta\lambda$ indicate that the TP effect reduces the thermal conductivity by ∼2-5% for the thermodynamics states investigated in this work. In all cases, S_{TP} carries the largest relative error. This result confirms the notion that fluids that become polarized under a thermal gradient become worse heat conductors.

IV. CONCLUSION

We have shown that thermal gradients applied to acetonitrile in the liquid and supercritical states induce thermal polarization. This is reflected in the build up of an electrostatic field between hot and cold regions. The strength of this thermal polarization field increases with the static dielectric constant and the reduction of temperature, showing the effect can be significant at near standard conditions, with a TP coefficient $S_{TP} \sim -0.6$ mV K^{-1}. Large temperature gradients, 10^{6-8} K m^{-1}, can be obtained using plasmonic systems[24], hence the effect could lead to measurable fields, 10^{2-5} V m^{-1}, opening a route to experimental observations of the TP effect at standard conditions. The TP effect might be relevant in thermo-plasmonics, where local polarization effects and the refractive index of the surrounding medium influence the plasmonic response.

We have shown that electrostatic fields of similar magnitude are obtained at near standard and supercritical conditions. The analysis of the phenomenological coefficients defining S_{TP} shows that at near standard conditions, large dielectric constants and the low temperatures are major factors in contributing to the field strength. In contrast, the TP strength at supercritical conditions is connected to the enhanced rotational diffusion, and the

stronger cross-coupling between the heat and polarization fluxes. At standard conditions, the TP electrostatic field is dominated by dipolar contributions, while higher order terms become the largest contributors for the supercritical fluid (as is the case for water[2]). Unlike the physical behaviour observed in water,[2] the TP field of aceotonitrile does not feature a reversal in sign.

We have demonstrated that the TP effect has a measurable impact on the thermal conductivity of polar fluids. We find that the coupling of heat and polarization fluxes leads to a reduction in thermal conductivity of ∼2-5%, both at near standard and supercritical conditions. While differences in thermal conductivities obtained from non-equilibrium and equilibrium simulation techniques might be masked by statistical uncertainties, these thermal conductivities must be different due the coupling of polarization and heat fluxes. Equilibrium approaches relying on linear response theory and Green-Kubo equations would thus need to include the cross coefficients to obtain reliable thermal conductivities, in a similar fashion to what has been done before[25,29] in equilibrium simulations of the Soret effect.

DATA AVAILABILITY

The data that support the findings of this study are available from the corresponding author upon reasonable request.

ACKNOWLEDGMENTS

We thank Prof. Fernando Moreno for helpful discussions, Imperial College London for the award of a Europeans Partner Fund grant, the EPSRC for the award of project EP/J003859/1, the Leverhulme Trust for grant RPG-2018-384, the Spanish Ministry of Science for project PGC2018-096649-B-I00, and EPSRC for a DTP PhD scholarship to ORG. P.A acknowledges funding for a Ramon y Cajal Fellowship RYC-2016-20831. We thank the ICL RCS High Performance Computing facility for providing computational resources.

REFERENCES

[1] F. Bresme, A. Lervik, D. Bedeaux, and S. Kjelstrup, "Water polarization under thermal gradients," Phys. Rev. Lett. **101**, 020602 (2008).

[2] I. Iriarte-Carretero, M. A. Gonzalez, J. Armstrong, F. Fernandez-Alonso, and F. Bresme, "The rich phase behavior of the thermopolarization of water: from a reversal in the polarization, to enhancement near criticality conditions," Phys. Chem. Chem. Phys. **18**, 19894–19901 (2016).

[3] C. D. Daub, P.-O. Åstrand, and F. Bresme, "Polarisation of polar dumbbell fluids in thermal gradients: the importance of the treatment of electrostatic interactions," Mol. Phys. **114**, 3249–3254 (2016).

[4] A. A. Lee, "Microscopic mechanism of thermomolecular orientation and polarization," Soft Matter **12**, 8661–8665 (2016).

[5] P. Wirnsberger, D. Fijan, R. A. Lightwood, A. Šarić, C. Dellago, and D. Frenkel, "Numerical evidence for thermally induced monopoles," Proc. Natl. Acad. Sci. U. S. A. **114**, 4911–4914 (2017).

[6] F. Römer, F. Bresme, J. Muscatello, D. Bedeaux, and J. M. Rubí, "Thermomolecular orientation of nonpolar fluids," Phys. Rev. Lett. **108**, 105901 (2012).

[7] A. Gardin and A. Ferrarini, "Thermo-orientation in fluids of arbitrarily shaped particles," Phys. Chem. Chem. Phys. **21**, 104–113 (2019).

[8] O. R. Gittus, J. D. Olarte-Plata, and F. Bresme, "Thermal orientation and thermophoresis of anisotropic colloids: The role of the internal composition," Eur. Phys. J. E **42**, 90 (2019).

[9] A. L. Garner, M. Deminsky, V. B. Neculaes, V. Chashihin, A. Knizhnik, and B. Potapkin, "Cell membrane thermal gradients induced by electromagnetic fields," J. Appl. Phys. **113**, 214701 (2013).

[10] K. Abe and K. Hyeon-Deuk, "Dynamical ordering of hydrogen molecules induced by heat flux," J. Phys. Chem. Lett. **8**, 3595–3600 (2017).

[11] R. J. W. Le Fèvre, B. J. Orr, and G. L. D. Ritchie, "Molecular polarisability. anisotropic polarisability of the cyanogroup from molar kerr constants and dipole moments of eight nitriles," J. Chem. Soc. , 2499–2505 (1965).

[12] D. P. Shelton, "Are dipolar liquids ferroelectric?" J. Chem. Phys. **123**, 084502 (2005).

[13] M. A. Pounds and P. A. Madden, "Are dipolar liquids ferroelectric? simulation studies," J. Chem. Phys. **126**, 104506 (2007).

[14] C. D. Wick, J. M. Stubbs, N. Rai, and J. I. Siepmann, "Transferable potentials for phase equilibria. 7. primary, secondary, and tertiary amines, nitroalkanes and nitrobenzene, nitriles, amides, pyridine, and pyrimidine," J. Phys. Chem. B **109**, 18974–18982 (2005).

[15] H. J. C. Berendsen and W. F. van Gunsteren, "Molecular dynamics simulations: Techniques and approaches," (Reidel, Dordrecht, The Netherlands, 1984) Chap. 8, pp. 475–500.

[16] G. D. Team, "Gromacs documentation: Release 2020," (2020).

[17] B. Hess, H. Bekker, H. J. C. Berendsen, and J. G. E. M. Fraaije, "Lincs: A linear constraint solver for molecular simulations," J. Comp. Chem. **18**, 1463–1472 (1997).

[18] T. Darden, D. York, and L. Pedersen, "Particle mesh ewald: An n log(n) method for ewald sums in large systems," J. Chem. Phys. **98**, 10089 (1993).

[19] M. J. Abraham, T. Murtola, R. Schulz, S. Páll, J. C. Smith, B. Hess, and E. Lindahl, "Gromacs: High performance molecular simulations through multi-level parallelism from laptops to supercomputers," SoftwareX **1–2**, 19–25 (2015).

[20] M. Parrinello and A. Rahman, "Polymorphic transitions in single crystals: A new molecular dynamics method," J. Appl. Phys. **52**, 7182–7190 (1981).

[21] G. Bussi, D. Donadio, and M. Parrinello, "Canonical sampling through velocity rescaling," J. Chem. Phys. **126**, 014101 (2007).

[22] G. A. Chapela, G. Saville, S. M. Thompson, and J. S. Rowlinson, "Computer simulation of a gas–liquid surface. part 1," J. Chem. Soc., Faraday Trans. 2 **73**, 1133–1144 (1977).

[23] A. O. Govorov, W. Zhang, T. Skeini, H. Richardson, J. Lee, and N. A. Kotov, "Gold nanoparticle ensembles as heaters and actuators: melting and collective plasmon resonances," Nanoscale Res. Lett. **1**, 84 (2006).

[24] C. R. Crick, P. Albella, B. Ng, A. P. Ivanov, T. Roschuk, M. P. Cecchini, F. Bresme, S. A. Maier, and J. B. Edel, "Precise attoliter temperature control of nanopore sensors using a nanoplasmonic bullseye," Nano Lett. **15**, 553–559 (2015).

[25] J. Armstrong and F. Bresme, "Thermal conductivity of highly asymmetric binary mixtures: how important are heat/mass coupling effects?" Phys. Chem. Chem. Phys. **16**, 12307–12316 (2014).

[26] R. J. Hulse, M. W. Anderson, M. D. Bybee, D. D. Gonda, C. A. Miller, J. L. Oscarson, R. L. Rowley, and W. V. Wilding, "Liquid thermal conductivities of acetonitrile, diethyl sulfide, hexamethyleneimine, tetrahydrothiophene, and tetramethylethylenediamine," J. Chem. Eng. Data **49**, 1433–1435 (2004).

[27] L. Qun-Fang, L. Rui-Sen, N. Dan-Yan, and H. Yu-Chun, "Thermal conductivities of some organic solvents and their binary mixtures," J. Chem. Eng. Data **42**, 971–974 (1997).

[28] J. V. Sengers, "Transport processes near the critical point of gases and binary liquids in the hydrodynamic regime," Ber. Bunsenges. Phys. Chem. **76**, 234–249 (1972).

[29] S. de Groot and P. O. Mazur, *Non-Equilbrium Thermodynamics* (North-Holland Publishing Co., Amsterdam, 1962).

[30] D. S. Venables and C. A. Schmuttenmaer, "Far-infrared spectra and associated dynamics in acetonitrile–water mixtures measured with femtosecond thz pulse spectroscopy," J. Chem. Phys. **108**, 4935–4944 (1998).

[31] A. Sugitani, S. ichi Ikawa, and S. Konaka, "Effect of temperature on the infrared band shapes and reorientational and vibrational relaxation of liquid acetonitrile," Chemical Physics **142**, 423 – 430 (1990).